This is life: some thoughts on self-organized structure formation in active liquids and biological systems

Hoffmann, L.A.

CHAPTER 4

Transition to Homochirality in Vicsek Model

Chirality is a feature of many biological systems and much research has been focused on understanding the origin and implications of this property. Most famously, sugars and amino acids that are found in nature are homochiral, meaning that chiral symmetry is broken and only one of the two possible chiral states is ever observed. Perhaps less well-know, something similar is the case for certain types of cells too. They show chiral behavior and only one of the two possible chiral states is observed in nature. Understanding the origin of cellular chirality and what, if any, use or function chirality has in tissues and cellular dynamics is still an open problem and subject to much (recent) research. Here, we develop a simple model to describe the possible origin of homochirality in cells. Combining the Vicsek model for collective behavior with the model of Jafarpour et al. [231], developed to describe the transition to homochirality for molecules, we investigate how a homochiral state might have evolved in cells from an initially symmetric state without any mechanisms that explicitly break chiral symmetry. We find that noise, both on the level of flocking and on the level of cell division, is an important factor determining if and when a homochiral state is reached. We study how the competition between cooperative behavior and noise affects the transition to homochirality as well as the influence of cell death and cell division rates.

L. A. Hoffmann and L. Giomi, *Transition to Homochirality in Vicsek Model.* In preparation.

[...] [K]nowledge simply does not exist in complete independence of power [...] [S]ystems of knowledge, although expressing objective (and perhaps even universally valid) truth in their own right, are nonetheless always more or less closely tied to the regimes of power that exist within a given society. Conversely, regimes of power necessarily give rise to bodies of knowledge about the objects they control, but this knowledge may — in its objectivity — go beyond and even ultimately threaten the project of domination from which it arises.

G. Gutting about M. Foucault. *French Philosophy in the Twentieth Century.*

[...] [T]he past should be altered by the present as much as the present is directed by the past.

T. S. Eliot. *Tradition and the Individual Talent.*

Chirality, the property of an object that cannot be superimposed onto its mirror image, is an important concept in physics and biology. For molecules, for example, one calls the two chiral states L- and D-molecules. Usually, chemical reactions produce molecules of both chirality in equal amounts, producing what is called a racemic mixture, where left-right symmetry is not broken. Thus, the production of these molecules does not seem to favor one chiral state over the other such that chiral symmetry is not explicitly broken during the production of molecules. Nevertheless, it is well known that in nature and biology homochiral states (only one of the two possible chiral states is present) are common. For example, most amino acids are L-molecules whereas most sugars are D-molecules. These smaller chiral molecules are the building blocks of larger molecules that in turn are also chiral. The question about the origin of the symmetry breaking and what its effects are in biological systems has been subject to many debates and studies, see, e.g., Refs. [232–236] and references therein. In particular, the question of which, if any, biological use a particular chirality has, or if the symmetry breaking is just random, is still hotly debated. While it is known that chirality seems to be crucial in small biological structures, where it was found to be linked to the function of e.g. proteins, it is less clear if and how chirality plays a role in larger biological structures. However, there has been some evidence that left-right (LR) asymmetry is crucial on these scales as well. Unlike for molecules or certain larger biological structures like swimming sperm cells [237, 238] or flagella of bacteria [239], the presence and role of chirality is not necessarily as obvious for eukaryotic cells. Nevertheless, recent work has shown that LR asymmetry plays an important role here as well, both for unicellular [235] and multicellular systems. For example, cell chirality has been shown to have an influence during morphogenesis in Drosophila [240], snails [241], *C. elegans* [242], or mammalian cells [122, 218]. In particular, in the context of active matter, where cells are modeled as active nematics [42, 49], it has been shown that the presence of chiral stresses on the level of the single cell modifies the dynamics on the level of tissues [138, 243]. However, the evolutionary origin of cellular chirality is still unclear. Different models of active matter have been successfully applied to describe cells. These models have in common that they describe large-scale properties, like flocking, of cell monolayers or tissues, rather than accurately model the microscopic dynamics of individual cells.

In this article we are investigating the possible origin of cellular homochirality and, in particular, we investigate how large-scale flocking might influence the transition to homochirality. For molecules, simple models have been proposed to explain how one might end up in a homochiral state starting from a racemic state without any explicit LR asymmetry. One example is the recent work by Jafarpour et al. [231, 236] who showed, using a minimal model of only two reaction equations, that the homochiral state can be the only fixed point of the dynamics if the noise inherent in the chemical reactions that are producing molecules is taken into account. That is, due to the presence of noise the LR symmetry is spontaneously broken and the system can reach a homochiral state from an initially racemic one, with the choice of which homochiral state is selected being random. We adopt a similar model to investigate the possible origin of homochirality in cells. Rather than being con-

cerned with the microscopic details, e.g. if there is a connection between chirality on the molecular level and chirality of cells, we adopt a simplified coarse-grained model of cells. The major difference between the molecules considered by Jafarpour et al., that undergo passive diffusion, and our approach is that we consider cells to be active, self-propelled particles that tend to align with their neighbors. This results in markedly different spatial dynamics. We numerically investigate if and how the presence of activity and alignment interactions influences the transition to homochirality from a racemic state. We find that for the right choice of model parameters the system is guaranteed to reach a homochiral state in a finite time. While the system is in a mixed state, that is away from homochirality, we find large fluctuations of the number density and the local chirality. Furthermore, we observe that particles of same chirality tend to be more correlated in space than particles of opposite chirality, even though there is no explicit interaction term favoring one over the other. Finally, we find that the time a given system takes to transition to homochirality follows a long-tail distribution, with mean and standard deviation being of the same order of magnitude.

In the following section we first describe our model in more detail. Afterwards, we investigate under which conditions the system transitions from a racemic to an homochiral state. Furthermore, we investigate spatial fluctuations and heterogeneities in the system. Finally, we consider in more detail the transition to homochirality, and how the transition time depends on several of the parameters of the model.

4.1 Model

Our model consists of two separate parts that are minimally coupled, one describing cell division and death, the other the spatial dynamics, namely collective motion and flocking, of cells. We first describe the two parts separately and afterwards explain how they are coupled in our simulations. We adopt a version of a stochastic model introduced originally by Frank [232] and expanded on by Jafarpour et al. [231, 236] recently. There are two kinds of reactions for the two chiral states:

$$F + R \xrightarrow{k_m} 2R\,, \qquad F + L \xrightarrow{k_m} 2L \tag{4.1a}$$

$$R \underset{k_c}{\overset{k_d}{\rightleftharpoons}} F\,, \qquad L \underset{k_c}{\overset{k_d}{\rightleftharpoons}} F\,. \tag{4.1b}$$

Here, R denotes right-chiral cells, L denotes left-chiral cells and F denotes nutrients; see also Fig. 4.1a. Thus, the first two equations, Eqs. (4.1a), simply describe cell division: A single cell consumes nutrients and divides into two cells with a rate k_m. The second set of equations, Eqs. (4.1b), contains a forward and a backwards reaction. The former, occurring with rate k_d, models cell death. A single cell decays into a nutrient. This reaction can be seen as an effective reaction consisting of two parts. In cell monolayers, for example, a cell that died will be extruded from the monolayer (cell apoptosis). New nutrients can then enter the system, effectively replacing, simplistically speaking, the dead cell. These two steps can be summarized as one effective reaction occurring with the rate k_d. The backwards reaction, occurring with rate k_c, appears to describe that cells are spontaneously created from

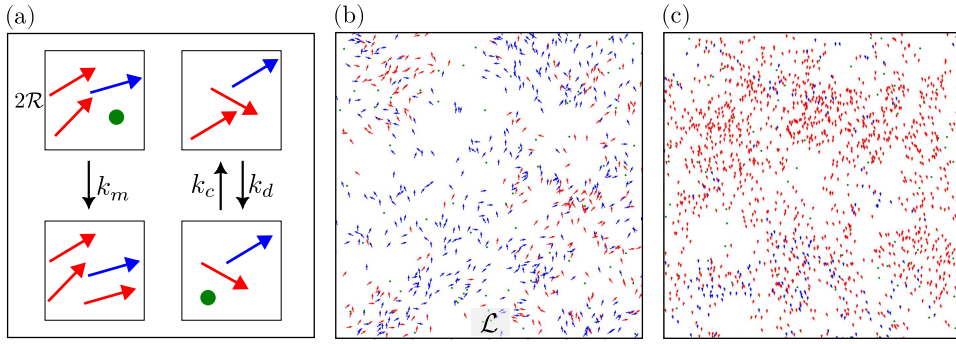

Figure 4.1: Model.

(a) A schematic of the reactions defined in Eqs. (4.1). To perform the reactions we subdivide the total system into square boxes of height $2\mathcal{R}$. Left-chiral particles (red arrow) and right-chiral particles (blue arrow) can divide with the rate k_m through the consumption of nutrients (green dot). Here a left-chiral particle divides. Furthermore, they die with the rate k_d and are replaced by a nutrient, or the nutrient "spontaneously transforms" into a particle with rate k_c. Here a left-chiral particle undergoes these reactions. See the main text for a proper interpretation of the rates. (b) Snapshot of the simulations carried out in a square system of height $\mathcal{L}$ at density $\rho = 2$ and noise $\eta = 0.3$. Again, right-chiral particles are represented by blue arrows while left-chiral particles are represented by red arrows. (c) A snapshot taken for higher densities ($\rho = 4$) and lower noise ($\eta = 0.1$).

nutrients. However, it is again better interpreted as an effective reaction that can be split into two parts. This reaction describes cells entering the system we are considering from an external reservoir. In the system they replace some of the nutrients that are present. The reaction rate k_c thus encodes the "openness" of the system we are considering. If the rate vanishes the system is closed and no cells can enter from outside, while if the rate is positive there is a non-vanishing flux of cells into the systems. While these interpretations perhaps do not accurately reflect the biologically processes occurring on the microscopic scale, we choose the reactions like this for two reasons: i) the simplicity of the reactions, capturing the main dynamics while ii) the total number $N = N_R + N_L + N_F$ of particles in the system is conserved by this choice of reactions, which simplifies the dynamics considerably. Thus, we have a model with three non-trivial reaction rates, k_m (division), k_d (death), and k_c (entering). Note that all of the reactions in Eqs. (4.1) are symmetric for left and right chirality, i.e., there is no explicit symmetry breaking.

We now explain to the Vicsek model, which we use to model the spatial dynamics of the cells. Since this model has been studied intensely over the last 25 years we keep the description here brief and refer to, e.g., Chapter 1 and Refs. [97, 99, 100] for a more in-depth explanation. The ith of $M = N_R + N_L$ self-propelled particles is located at position $\boldsymbol{r}_i(t)$ at time t and it has an orientation $\boldsymbol{p}_i(t) = (\cos\theta_i(t), \sin\theta_i(t))$. Each particles moves with constant speed v_0 in the direction of their orientation. Additionally, a given particle tends to align its orientation with the average orientation of all neighboring particles that are closer than a distance $\mathcal{R}$ to

this particle. Additionally, there is some rotational noise perturbing this alignment interaction. This results in the following time-discrete equations of motion:

$$\boldsymbol{r}_i(t+\Delta t) = \boldsymbol{r}_i(t) + \Delta t v_0 \boldsymbol{p}_i(t+\Delta t) \tag{4.2}$$

$$\theta_i(t+\Delta t) = \arg\left[\sum_j C_{ij}(t)\boldsymbol{s}_j(t)\right] + \eta\xi_i(t)\ , \tag{4.3}$$

where $C_{ij}(t)$ is the connectivity matrix whose entries are $C_{ij}(t) = 1$ if $|\boldsymbol{r}_i(t) - \boldsymbol{r}_j(t)| < \mathcal{R}$ and $C_{ij}(t) = 0$ if $|\boldsymbol{r}_i(t) - \boldsymbol{r}_j(t)| > \mathcal{R}$. $\xi_i(t)$ is a Gaussian white noise with zero average and unit variance. The parameter η determines the importance of noise relative to alignment and in our convention $0 < \eta < 1$ such that $\eta = 1$ corresponds to effectively random reorientation after each time step and alignment is not important, i.e., the particles undergo active Brownian motion. If, on the other hand, η is sufficiently small and the density of particles is sufficiently large this results in a phase transition to a flocking state. The left- and right-chiral particles are subject to these dynamic equations while the nutrient particles are static and are not assigned an orientation.

We couple the two models as follows: After each time step of the Vicsek model we divide the total system into boxes of area $(2\mathcal{R})^2$ and let the stochastic model Eq. (4.1) run in each of these boxes for m steps. We simulate these reactions using a Gillespie algorithm [244, 245]. After updating the population in each box according to the reactions we perform another time step of the Vicsek model. The system we consider is two-dimensional square box of height $\mathcal{L}$, with periodic boundary conditions imposed. We initialize the system with one randomly positioned and oriented left-chiral and one right-chiral particle, each. At a given density ρ there are then $N_F(t=0) = \rho\mathcal{L}^2$ number of nutrient particles. Thus, the total number of particles in the system for a given density ρ is given by $N(t) = N = \rho\mathcal{L}^2 + 2$ which, as explained above, is conserved and constant in time by construction. We fix length scales by setting the interaction radius to unity, $\mathcal{R} = 1$, and time scales by setting the time step in the Vicsek model to unity, $\Delta t = 1$. Furthermore, we fix $k_d = 10$ and define $\tilde{k}_m = k_m/k_d$ and $\tilde{k}_c = k_c/k_d$. In the following we will always work with the rescaled rates, but drop the tilde. The effect of varying the other model parameters will be investigated below. In Figs. 4.1b,c we show a snapshot of the simulations at different densities and values of N_L/N_R. While the global alignment in Fig. 4.1b is low, for higher values of density and lower values of noise almost all particles have the same orientation in Fig. 4.1c. We color left-chiral particles red and right-chiral particles blue. Note that the latter system shown in Fig. 4.1c is considerably closer to homochirality than the former, with $N_L \gg N_R$. The question whether the density and flocking has an effect on the appearance of homochirality or the mean time until this state is reached will be discussed below.

4.2 Results

We now present the results of our analysis of the described model. First, we investigate the effect of the rate k_c. As we will see, the system is guaranteed to reach a

homochiral state only if this rate vanishes. Therefore, as we are interested in the transition to homochirality, we afterwards set $k_c = 0$ and instead investigate the time it takes a given system on average to reach the homochiral state. We investigate how varying different model parameters speeds up or slows down the transition time.

4.2.1 Finite creation rate

As mentioned above, we interpret the rate k_c as the rate with which new cells of either chirality are introduced into the system but not as a result of cell division. The most likely scenario for this to happen is for cells from outside the system we are considering to enter it, thereby replacing (consuming) nutrients that were present in the system before; i.e. there is a non-vanishing flux of cells into the system. This is assumed to happen equally likely for cells of either chirality, therefore guaranteeing that chiral symmetry is not explicitly broken. To study the effect of the rate k_c on the chirality of the system we first consider the global chirality of the system for different values. To this end we define the chiral order parameter as

$$\omega := \frac{N_L}{N_L + N_R} \in [0, 1] \tag{4.4}$$

such that $\omega = 0$ if no left-chiral particles are present, $N_L = 0$, and $\omega = 1$ if no right-chiral particles are present, $N_R = 0$. At these values of the order parameter the system is thus in a homochiral state. We now consider the probability distribution ω after a given number of time steps of the Vicsek model when the average of many independent runs has approximately reached a steady state. To obtain the probability distribution we record the order parameter at this time for 1000 independent simulations. This way we find the probability for a system to achieve a certain value of the order parameter for a given value of k_c. The resulting distributions are shown in Fig. 4.2 for some values of k_c. If k_c vanishes we find a bimodal probability distribution which takes non-vanishing values only at the homochiral states $\omega = 0$ and $\omega = 1$, see Fig. 4.2a. That is, the system always ended up in a homochiral state. It is equally likely to end up in a left-chiral or a right-chiral state, reflecting the fact that there is no explicit LR-symmetry breaking. While it is thus not possible to predict which of the two possible homochiral states a given system evolves to, it is, however, guaranteed to reach one of the two states in a finite time. The time evolution of the order parameter for some of the runs is presented in the inset. As can be seen, the order parameter heavily fluctuates initially, but once a system has evolved into a homochiral state it remains in this state. This reflects the fact that, for $k_c = 0$, once $N_L = 0$, new left-chiral particles cannot be created from the reactions Eqs. (4.1). The only reactions occurring for $N_L = 0$ are cell division and death of right-chiral particles. Similarly for $N_R = 0$. Thus, the homochiral states are a fixed point of the reactions if $k_c = 0$.

If the creation rate is finite, however, the system is not guaranteed to reach a homochiral state. In fact, we find that already for small values of k_c the probability distribution changes dramatically, with a system usually no longer reaching a homochiral state at all and the distribution being peaked at the racemic state $\omega = 0.5$

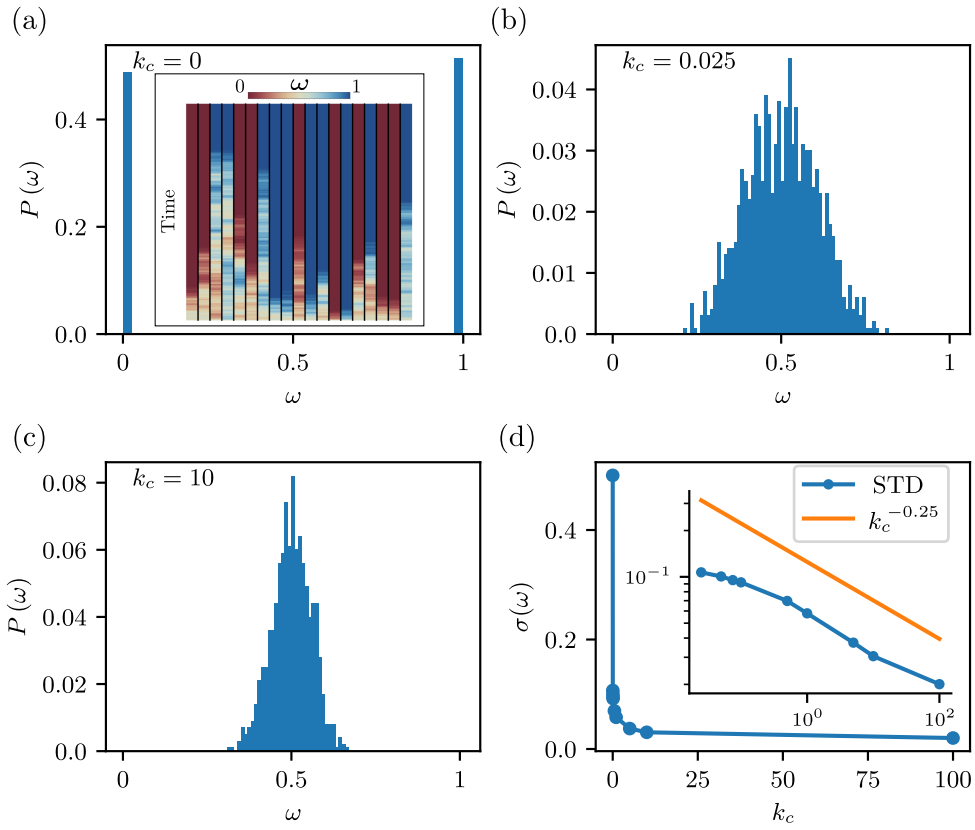

Figure 4.2: Distributions of global order parameter.

(a) Probability distribution $P(\omega)$ of the order parameter ω for vanishing rate k_c. The system is guaranteed to evolve to a homochiral state, thus $\omega = 0$ and $\omega = 1$ both occur with a probability of about 50%. The inset represents the time evolution of the order parameter for twenty independent runs. Each of the columns is an independent run and time increases in positive y-direction. The color code is according to the legend at the top, i.e., $\omega = 0$ (homochirality of right particles) is red, $\omega = 1$ (homochirality of left particles) is blue, the racemic state $\omega = 0.5$ is white. Every systems is initialized in a state with $\omega = 0.5$. The order parameter can be seen to fluctuate in time but eventually all systems evolve to one of the two homochiral states. (b) Probability distribution of the order parameter for $k_c = 0.025$. (c) Distribution for $k_c = 1$. (d) Distribution for $k_c = 10$. To obtain each of the histograms we measure the order parameter of the system after a certain number of time steps Δt, where the system has on average reached a stationary state, and average over 1000 independent runs. (d) We plot the standard deviation $\sigma(\omega)$ of the distribution $P(\omega)$ as a function of the reaction rate k_c. We find that the curve is well approximated by a power law decay with exponent -0.25 (see inset for log-log plot of standard deviation $\sigma(\omega)$ over k_c). Simulation parameters: $k_m = 5$, $\rho = 2$, $\eta = 0.3$, $v_0 = 0.4$, $m = 2$.

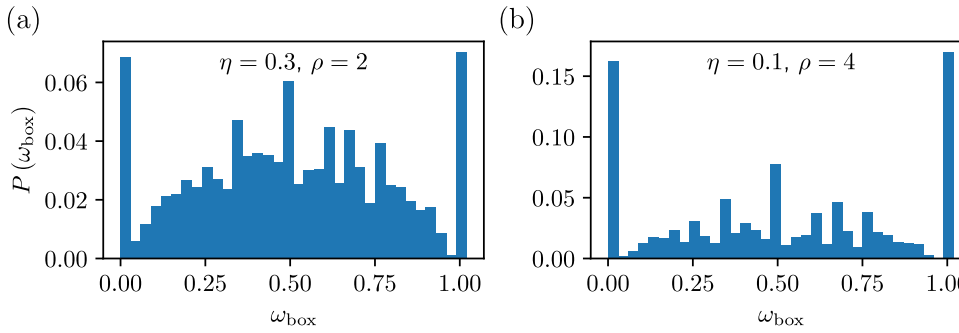

Figure 4.3: Distributions of local order parameter.

We measure the local order parameter ω_{box}, that is the order parameter in each of the square boxes of height $2\mathcal{R}$. Per system there are $(\mathcal{L}/2\mathcal{R})^2 = 100$ boxes. To obtain the histograms we show here we average over 1000 independent runs. If a box is empty the order parameter is not well defined and we do not include it in the histogram. (a) The probability distribution for noise $\eta = 0.3$ and density $\rho = 2$. (b) The probability distribution for noise $\eta = 0.1$ and density $\rho = 4$. Simulation parameters: $k_c = 0.025$, $k_m = 5$, $v_0 = 0.4$, $m = 2$.

4

(see Fig. 4.2b for $k_c = 0.025$). As k_c increases, the width of the probability distribution decreases rapidly (see Fig. 4.2c for $k_c = 1$), and for large values of k_c the distribution is sharply peaked around $\omega = 0.5$ (Fig. 4.2d for $k_c = 10$). To quantify this behavior we computed the standard deviation $\sigma(\omega)$ of the distributions as a function of the rate k_c over four orders of magnitude. We find that approximately $\sigma(\omega) \sim k_c^{-1/4}$. Lastly, note that the distribution is symmetric for all values of k_c, reflecting that the fact that there is no mechanism that explicitly breaks the chiral symmetry. The average order parameter is always $\langle\omega\rangle = 0.5$. On the other hand, if initially there were more cells of one chirality in the system this would heavily skew the final results and break symmetry (not shown here).

So far we have only considered global properties of the system (namely the global order parameter). We now turn towards studying some local properties, namely the spatial variation of the order parameter as well as number density fluctuations and number density correlation functions. Above we presented the results for the order parameter ω which is obtained from averaging over the entire system. However, as is already evident from the simulations of the snapshots in Figs. 4.1b,c, the order parameter and particle density are not homogeneous but instead vary greatly in space. The inhomogeneity of the order parameter is due to the anisotropy introduced through the alignment interaction in the Vicsek model.

To investigate how the order parameter varies in space we choose $k_c = 0.025$ as an example. Instead, we consider one case of higher noise ($\eta = 0.3$) and lower density ($\rho = 2$) as well as one case of lower noise ($\eta = 0.1$) and higher density ($\rho = 4$). The latter is deep in the flocking regime (see snapshot Fig. 4.1c), while for the former the overall alignment of particles is lower (see snapshot Fig. 4.1b). We present in Fig. 4.3 the histogram that we obtain as follows. At the end of the run we measure the order parameter ω_{box} in every box of size $\mathcal{R}^2$ of the system.

We only include the order parameter in the histogram if this box is not empty, i.e., contains at least one left- or right-chiral particle, such that the order parameter is well defined. The histogram is then obtained from averaging over all independent runs. We find that this probability distribution is strongly peaked around $\omega_{\mathrm{box}} = 0$ and $\omega_{\mathrm{box}} = 1$, and that there is another maximum at $\omega_{\mathrm{box}} = 0.5$. The relatively non-monotonic shape of the histogram, can be explained by some values of $\omega_{\mathrm{box}} = 0$ being much more likely to occur if they are rational numbers for ratios of small number of particles. This is particularly evident for small densities where only few particles are present in some boxes. However, in either case we find the general trend of the distribution decreasing away from $\omega_{\mathrm{box}} = 0.5$, and then strongly increasing at the edges. A noticeable difference between the two cases shown in Fig. 4.3 is that for higher densities and lower noises the relative height of the homochiral points is much lower. We have also considered an intermediate state of lower noise ($\eta = 0.1$) and lower density ($\rho = 2$) (not shown) and did not find a significant difference from the histogram in Fig. 4.3a. thus, we conclude that it is mainly a density effect.

In Figs. 4.4a,b we present the probability distribution of finding a number n^R_{box} of right-chiral particles in a given system. Here, we define n^R_{box} as the number of right-chiral particles in a given box. As the distribution for left- and right-chiral particles is essentially identical, we only show one of the two. Again, we consider the average over independent runs at a fixed time where the average over all system has reached a steady state to find the probability distributions. Note that if all particles were distributed homogeneously in space, $\langle n_{\mathrm{box}} \rangle_{\mathrm{hom}} = (2\mathcal{R})^2 \rho$. We normalize the number of particles by this number and write the renormalized quantities with a tilde, i.e., $\tilde{n}^R_{\mathrm{box}} = n^R_{\mathrm{box}} / \langle n_{\mathrm{box}} \rangle_{\mathrm{hom}}$. For $k_c = 0$, i.e., if the system is in the homochiral state at the time of measurement, the probability of finding no right-chiral particles at all is around 50%, reflecting the fact that half the systems we average over are filled only with left-chiral particles (inset in Fig. 4.4a). If we look at the distribution without the cases where left-homochirality exists, the distribution is rather broad, see Fig. 4.4a, with a mean of $\langle \tilde{n}^R_{\mathrm{box}} \rangle \approx 0.9$ particles per box with relative fluctuations of $\sigma\left(\tilde{n}^R_{\mathrm{box}}\right) / \langle \tilde{n}^R_{\mathrm{box}} \rangle \approx 0.62$, where $\sigma\left(\tilde{n}^R_{\mathrm{box}}\right)$ is the standard deviation of the distribution. Note that the distribution peaks at $\tilde{n}^R_{\mathrm{box}} = 0.75$ and decreases for both smaller and larger values. If we consider the total number of particles $\tilde{n}_{\mathrm{box}}$ without regard for their chirality, that is $\tilde{n}_{\mathrm{box}} = \tilde{n}^R_{\mathrm{box}} + \tilde{n}^L_{\mathrm{box}}$, we find the distribution shown in Fig. 4.4b. It is essentially identical to the one for right-chiral particles (after subtraction of the systems where left-homochirality is present), reflecting the fact that we the system is always in a homochiral state, thus either only right- or only left-chiral particles are present, and their distribution is equal to the distribution of all particles. This is markably different for non-vanishing k_c. Again, we choose $k_c = 0.025$ as an example. The most likely case now is to encounter a box that contains no right-chiral particles and the distribution is monotonically decreasing for increasing $\tilde{n}^R_{\mathrm{box}}$, see Fig. 4.4c. The average $\langle \tilde{n}^R_{\mathrm{box}} \rangle \approx 0.46$ is about half the previous average value (reflecting that the mean global order parameter is $\omega = 0.5$), but the distribution is much wider, with the standard deviation almost being equal to the mean, $\sigma\left(\tilde{n}^R_{\mathrm{box}}\right) / \langle \tilde{n}^R_{\mathrm{box}} \rangle \approx 0.99$. Thus, fluctuations are very large. The distribution for the total number of particles in this

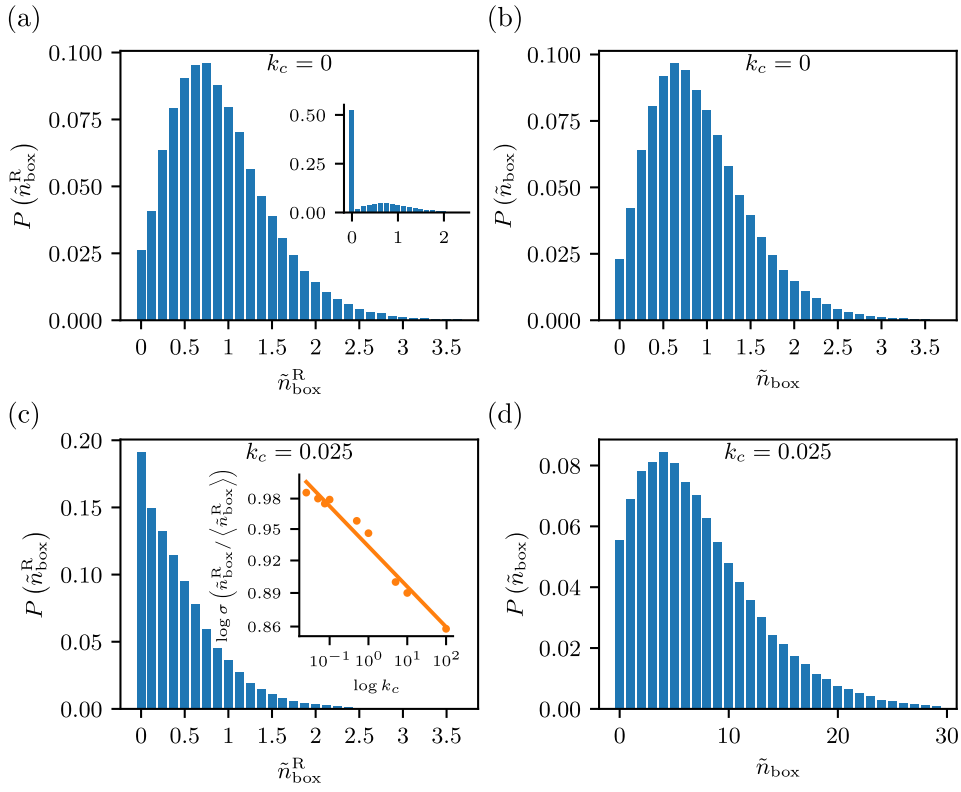

Figure 4.4: Fluctuations of particles density.

(a) We show the probability distribution to find a number of $\tilde{n}^R_{\mathrm{box}}$ right-chiral particles in a box for $k_c = 0$. Here, $\tilde{n}^R_{\mathrm{box}}$ is not the total number of particles but the ratio of number of particles over the average number of particles one would expect in a box in a homogeneous system (see main text). Thus for $\tilde{n}^R_{\mathrm{box}} < 1$ the number of particles in a box is smaller than expected in a homogeneous system while for $\tilde{n}^R_{\mathrm{box}} > 1$ it is greater. The probability distribution shown here is obtained by ignoring/subtracting the cases where the system has evolved to a left-homochiral state. The inset shows the distribution if these cases are not subtracted. The large probability of finding a box without right-chiral particle reflects the fact that the system evolves in half of the runs to a left-homochiral where no right-chiral particles are present. (b) The probability to find a given relative total number of particles in a box. (c) The same probability distribution as in (a) but for $k_c = 0.025$ and without subtracting the cases of left homochirality. This is because, as was shown in Fig. 4.2, the system virtually never evolves to a homochiral state and the systems are always mixed. The inset shows the depends of the ratio of standard deviation over mean for the probability distribution $P(\tilde{n}^R_{\mathrm{box}})$ as a function of the rate k_c. The best fit is found to be $\sim k_c^{0.017}$. (d) The same distribution as in (b) but for $k_c = 0.025$.

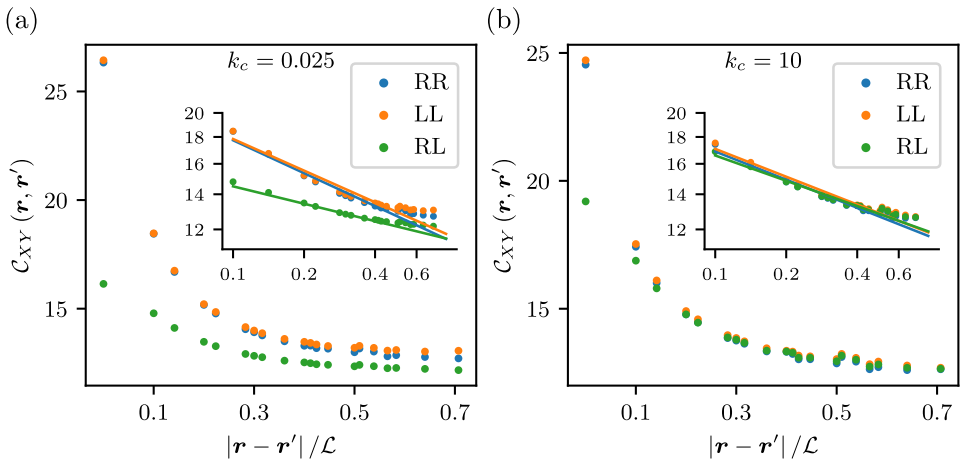

Figure 4.5: Correlations of particles density.

(a) The correlation function between right-chiral particles (RR, blue), left-chiral particles (LL, orange), and between left- and right-chiral particles (RL, green). The x-axis is distances measured in terms of the system size $\mathcal{L}$. The inset shows the same data in a log-log plot with the best fit of the linear region (in the log-log plot), namely $0.1 < |\boldsymbol{r}-\boldsymbol{r}'|/\mathcal{L} < 0.5$. (b) The same data but for $k_c = 10$ now. Simulation parameters: $k_m = 5$, $\rho = 2$, $\eta = 0.3$, $v_0 = 0.4$, $m = 2$. Again for each set of parameters we average over 1000 independent runs.

case (Fig. 4.4d) is similar to the one for vanishing rate k_c, with $\langle \tilde{n}_{\text{box}} \rangle \approx 0.9$ and $\sigma(\tilde{n}_{\text{box}})/\langle \tilde{n}_{\text{box}} \rangle \approx 0.75$. However, it is thus not anymore the same distribution as the right- or left-chiral distribution, as can be appreciated immediately by comparing Fig. 4.4c and Fig. 4.4d. With increasing k_c, the shape of the distribution remains similar, but $\langle \tilde{n}^R_{\text{box}} \rangle$ slightly increases (to $\langle \tilde{n}^R_{\text{box}} \rangle \approx 3.7$ for $k_c = 10$), while the relative fluctuations slightly decrease (see inset of Fig. 4.4c). Mean and relative fluctuations for the total number of particles $\tilde{n}_{\text{box}}$ remains constant. For $k_c = 0.025$, but higher density and lower noise ($\rho = 4$ and $\eta = 0.1$ compared with $\rho = 2$ and $\eta = 0.3$ before) we find that the shape of the distribution is not modified significantly, with the mean being equal, but that the distribution is slightly less broad, $\langle \tilde{n}^R_{\text{box}} \rangle \approx 0.84$ and $\langle \tilde{n}_{\text{box}} \rangle \approx 0.61$.

Apart from the number fluctuations for left- and right-chiral particles we can investigate their correlations in space. This is shown for two different values of k_c, $k_c = 0.025$ and $k_c = 10$, in Figs. 4.5a and Fig. 4.5b, respectively. We consider the spatial correlation function of the particles density $\mathcal{C}_{XY} = \langle n_X(|\boldsymbol{r}|)\, n_Y(|\boldsymbol{r}'|) \rangle$ for particles of same chirality ($X = Y = L$ or $X = Y = R$), and particles of different chirality, $X = R$ and $Y = L$. We find that, for $k_c = 0.025$ particles of same chirality are more strongly correlated in space than particles of different chirality, even on long distances, see Fig. 4.5a. Furthermore, the correlation functions follow approximately a power-law behavior with the decay for the correlation for particles of same chirality being about twice as large compared with the one for the correlation of different-

chirality particles. Namely, for $k_c = 0.025$, the same-chirality correlation function scales as $\mathcal{C}_{XX} \sim |\boldsymbol{r} - \boldsymbol{r}'|^{-0.2}$ while for the different-chirality correlation function $\mathcal{C}_{RL} \sim |\boldsymbol{r} - \boldsymbol{r}'|^{-0.11}$, see inset in Fig. 4.5a. For higher density and lower noise we find that the behavior is similar, with the ratio of the exponents being about two as well. For higher k_c, the correlation of the particle density of same chirality particles and different chirality particles overlaps is equal for large distances. Their power law behavior is very similar, with $\mathcal{C}_{XX} \sim |\boldsymbol{r} - \boldsymbol{r}'|^{-0.18}$ and $\mathcal{C}_{RL} \sim |\boldsymbol{r} - \boldsymbol{r}'|^{-0.16}$, see Fig. 4.5b. Furthermore, in this case the large length-scale behavior of the correlation functions is very similar as well.

We conclude this section with a brief summary of the results presented so far. In general, we find a large amount of inhomogeneity in number of particles and order parameter. This is despite the fact that our dynamical model for the motion in space (Vicsek model) does not distinguish between particles of different chirality. That is, the equations of motion for both species are identical and interaction between particles of same and different chirality are identical as well. Having studied the interaction properties of mixed systems, we now consider homochiral systems more closely. In particular, we are interested in the transition from a mixed to a homochiral state. Thus, in the following we always set $k_c = 0$ to guarantee that the system reaches a homochiral state in a finite time. That is, in all of the simulations below the probability distribution of the order parameter is peaked at $\omega = 0, 1$ and symmetric. Thus, instead of the order parameter we now investigate the *time* τ it takes a system with a given set of parameter values to reach the homochiral state. We vary different parameters to investigate how τ depends on them. We study its average $\langle \tau \rangle$ as well as the probability distribution $P(\tau)$.

4.2.2 Time to homochirality

To investigate the time it takes the system on average to reach the homochiral state we again run 1000 independent simulations, terminating each run only when a homochiral state is present. As explained above, for $k_c = 0$ the system is guaranteed to remain in a homochiral state once it has reached it and it is possible to end the simulation at this time. First, we consider the influence of the magnitude of rotational noise η of the Vicsek model on the transition to homochirality. We find that for small noises the mean time $\langle \tau \rangle$ required to reach the homochiral state is significantly larger than for lower noises and quickly decreases as noise is increased. On the other hand, the mean time for moderate and large noises is very similar, see Fig. 4.6a, with the mean time sometimes increasing very slightly for large noises. This is due to a small noise speeding up the time in which a particle can explore the space. In the extreme case of vanishing noise the initial particles remain on a single straight trajectory (possible due to the periodic boundary conditions), and the system remains occupied mainly by nutrients forever. Thus, a small noise is necessary to reach a homochiral state. However, increasing the noise more does not change the dynamics significantly. Remember that, while there is flocking at smaller noises, at large noises orientational alignment breaks down, Thus, perhaps surprisingly, flocking does not seem to speed up (or slow down) the transition to homochirality. For a better idea of the statistics we show in Fig. 4.6b the probability

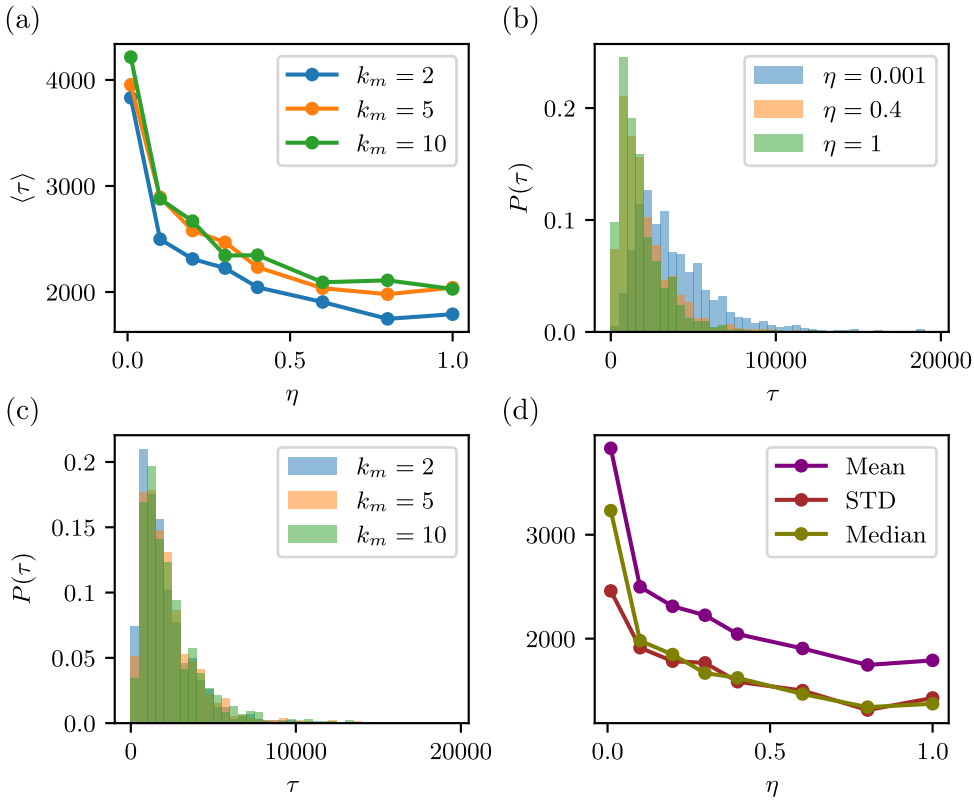

Figure 4.6: Transition time for different noise values and division rates.

(a) The average time $\langle\tau\rangle$ in which the system evolves for a homochiral state as a function of noise η for different cell division rates k_m. (b) The distribution $P(\tau)$ of the transition time τ found from recording τ for 1000 independent runs for three values of noise. (c) The same distribution but now for three different division rates. (d) The mean (purple), standard deviation (STD, red), and median (olive green) of the distribution $P(\tau)$ for different values of noise and for one division rate, $k_m = 5$. Simulation parameters: $k_c = 0$, $\rho = 2$, $v_0 = 0.4$, $m = 2$.

distributions for the time for a few different values of noise. We find that for all values of noise the distribution is peaked at small times but that that there is a significant tail. Thus, there is large diversity in the run times. Furthermore, we find a power-law behavior with $\langle\tau\rangle \sim \eta^{-0.16(\pm0.01)}$. However, since $\eta = 1$ is the maximal noise in our parametrization with orientations being randomly chosen in each time step for this value, the the noise is restricted to the values $\eta \in [0, 1]$, and thus it is not possible to study if the apparent power-law behavior persists over more than one order of magnitude. Thus, interestingly, a small amount of noise being present speeds up the transition to homochirality significantly.

Next, we consider different values for the cell division rate k_m. Remember that the rate k_m is defined relative to the death rate such that $k_m > 1$ is required for a growing cell population (greater division than death rate) and that for $k_m < 1$ the cells in a given system will eventually all die. Surprisingly, the value of the ratio is rather irrelevant, with the mean length for $k_m = 2$ and $k_m = 10$ being very similar even though in the former case the cells are dying at a rate five times higher, see Fig. 4.6a. In particular, different rates show the same power law behavior. To illustrate the similarity of the three different ratios we consider, we present in Fig. 4.6c the probability distribution for different rate ratios at a fixed noise. Indeed, they are almost indistinguishable. We find that these probability distributions are again strongly peaked at small times, but that there is a long tail with some runs taking almost five times the average time to reach homochirality. To quantify the probability distribution of the time to homochirality we present the mean, standard deviation, and median for a fixed rate ratio $k_m = 5$ for different noises. Note that the results for $k_m = 2$ and $k_m = 10$ is almost identical. We find that all three quantities have a similar magnitude and fall off at a similar rate, with the standard deviation and mean curves overlapping while the mean is shifted by a constant factor with respect to these curves, see Fig. 4.6d. All three curves follow the same power-law behavior $\sim \eta^{-0.16(\pm0.03)}$.

We now vary the two different speeds that are present in the system, namely the speed of movement v_0, entering through the Vicsek model, with which cells move in space as well as the speed of the reactions, namely how many times we run the Gillespie algorithm for between each time step Δt of the Vicsek model, i.e., the number of steps m. For both parameters we perform an analysis similar as the one for the noise presented above. Varying the speed v_0 we find that τ decreases with increasing speed, see Fig. 4.7a. The decrease is fast for low values of speed and slower for large values. The higher the speed the more peaked the distribution at small times. Again, we find that standard deviation and median curves are very similar but with the curve of the mean time $\langle\tau\rangle$ offset by a constant, such that all three quantities show the same power law behavior, namely $\langle\tau\rangle \sim \sigma(\tau) \sim v_0^{-0.25(\pm0.02)}$ (inset in Fig. 4.7a). A similar behavior is found when varying the number of steps m. The higher the number of steps the faster a homochiral state is reached, see Fig. 4.7b. The most significant difference compared with the speed v_0 is that the decay is much steeper as $\tau \sim m^{-0.64(\pm0.02)}$, see Fig. 4.7b.

Finally, we consider the effect of density on the transition time. For each value of density we again consider the different values of noise we have been studying before.

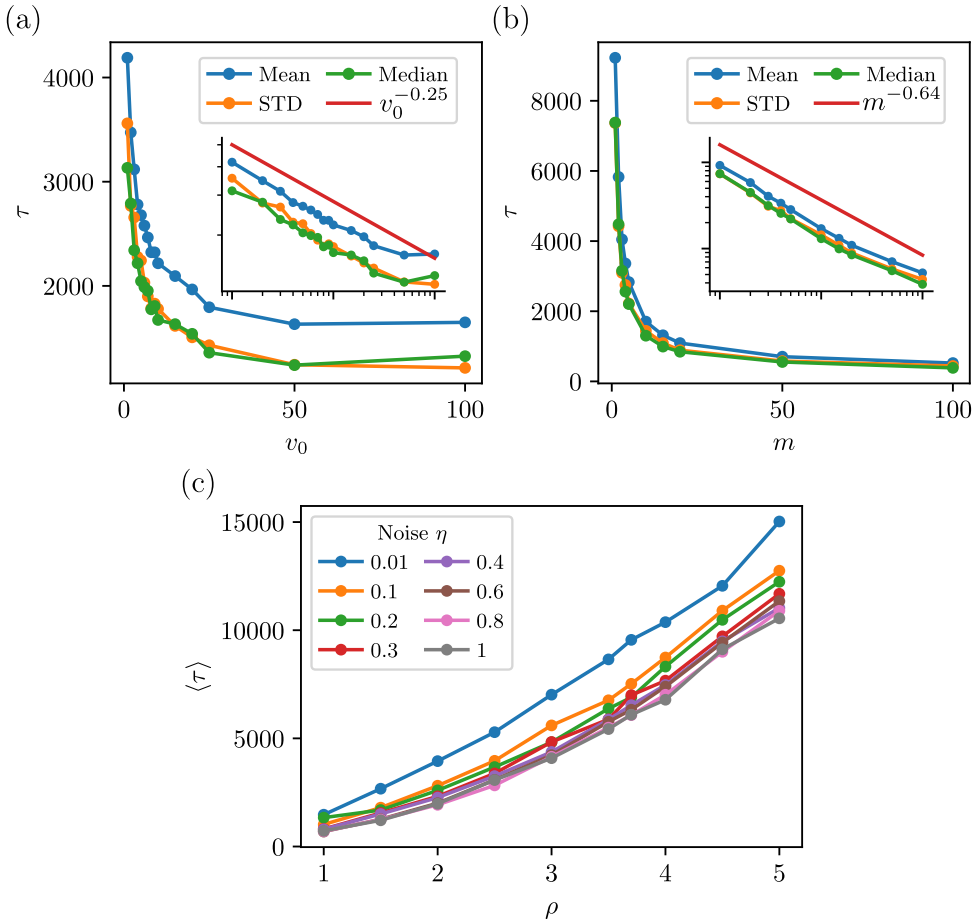

Figure 4.7: Transition time for different speed and density

(a) The mean (blue), standard deviation (STD, orange), and median (green) of the distribution $P(\tau)$ for different values of the speed v_0 of the Vicsek model. The inset shows the same data but in a log-log plot, with the red line indicating the power law decay of all three quantities $\sim v_0^{-1/4}$. (b) The data as in panel (a) but when varying m, the number of steps of the reactions performed during each step of the Vicsek model. Mean, standard deviation, and median now decay as $\sim x^{-0.64}$. (c) The average time $\langle\tau\rangle$ as a function of the density ρ. Each curve corresponds to a different values of noise η. Simulation parameters: $k_c = 0$, $k_m = 5$, $\rho = 2$ (in panels (a) and (b)), $v_0 = 0.4$ (in panels (b) and (c)), $m = 2$ (in panels (a) and (c)).

These two parameters, density and noise, are the crucial parameters when studying the flocking transition in the Vicsek model. We find that as we increase the density, the mean time increases slightly faster than linear for all values of η. Away from the smallest noise value $\eta = 0.01$, we do not find a significantly different behavior when varying the noise at a fixed density, see Fig. 4.7c.

Lastly, we note that when increasing $\mathcal{R}$, the mean time increases approximately linearly with $\mathcal{R}$, however the value of the noise becomes less important, with the time being considerably less sensitive to changes in noise, as expected since the alignment interaction radius is increased.

4.3 Discussion

We now deliver a more detailed discussion of some of our results. Jafarpour et al. [231, 236] used Eqs. (4.1) to describe a model that can explain the transition to homochirality in molecules. To account for spatially extended systems, they included a reaction equation that described molecules moving to a different neighboring box with a certain rate, thus molecules are effectively diffusive. Indeed the authors showed that a system governed by these discrete reaction equations can be described by the following continuous stochastic differential equation for the chiral order parameter ω:

$$\frac{\mathrm{d}\omega}{\mathrm{d}t} = -\frac{2Vk_ck_d}{Nk_m}\left(\omega - \frac{1}{2}\right) + \mathcal{D}\nabla^2\omega + \sqrt{\frac{2k_d}{N}\omega\,(1-\omega)}\zeta(t)\,, \tag{4.5}$$

where $N \gg 1$ is the number of particles, V the volume of the system, $\mathcal{D}$ a diffusion coefficient, and $\zeta(t)$ a Gaussian white noise of zero mean and unit variance. The noise $\zeta(t)$ is independent of our noise $\xi(t)$ included in the Vicsek model and is due to the inherent noise of the reaction equations. To explain why the system always reaches a homochiral state if k_c vanishes, we first consider a system that is not spatially extended, i.e., diffusion is irrelevant and the equation reduces to

$$\frac{\mathrm{d}\omega}{\mathrm{d}t} = \sqrt{\frac{2k_d}{N}\omega\,(1-\omega)}\zeta(t) \tag{4.6}$$

for $k_c = 0$. Note that this equation has two fix points, namely $\omega = 0$ and $\omega = 1$, that are the states of homochirality. Furthermore the relevant term on the right-hand side is coupled to the noise $\zeta(t)$. Thus, the reason the system ends up in the homochiral state is the presence of noise in the reactions and without it the homochiral states would not be fix points. Hence, Jafarpour et al. speak of noise-induced homochirality. The authors then show that including the diffusion term does not change the picture, thus the system described by

$$\frac{\mathrm{d}\omega}{\mathrm{d}t} = \mathcal{D}\nabla^2\omega + \sqrt{\frac{2k_d}{N}\omega\,(1-\omega)}\zeta(t) \tag{4.7}$$

has fix points at the homochiral state, and the system will evolve to these states in a finite time. We now adapt this argument to the extended model we studied.

The reactions described in Eqs. (4.1) are identical, however, the spatial dynamics is more complicated. Spatial dynamics is due to the Vicsek model, not simple diffusion. Thus, the second term on the right-hand side of Eq. (4.7) is still valid for our system, while the first has to be modified. A complete derivation of the continuous equations of motion describing our system is beyond the scope of this study. However, our observation of always finding a homochiral state if $k_c = 0$ can be explained as follows. Instead of diffusive dynamics our particles follow the Vicsek model, that is, they undergo persistent, anisotropic motion that is interrupted by rotational noise and alignment interactions. In the limit of $\eta \to 1$ we recover the case of active Brownian particles, which move isotropically through space. Thus, in this extreme case one can define an effective diffusion coefficient such that the form of Eq. (4.7) is unchanged, thus explaining why we still find the transition to homochirality. Away from the extreme case $\eta = 1$, the motion is no longer isotropic, thus the scalar factor in Eq. (4.7) has to be replaced by a matrix describing the anisotropic motion and alignment. However, this does not change the relevant structure of the equation and a similar argument as before can be applied for why a homochiral state is always reached in a finite amount of time.

4.4 Conclusion

We studied the Vicsek model coupled to a set of reaction equations that model cell division, cell death, and an influx of cells from outside the system. We found that the system is guaranteed to evolve to a homochiral state from an initially symmetrically mixed state in finite time only if the system is closed in the sense that the reaction rate k_c vanishes. In the mixed state we find large fluctuations of the local order parameter and the particle density around the mean value. In particular, we find that particles of same chirality tend to be correlated more strongly in space than particles of opposite chirality. In the case where the system evolves to a homochiral state, we showed that the transition time has a fat-tail distribution with ratio of mean and standard deviation being of order unity. Introducing a small amount of noise in the spatial dynamics significantly decreases the mean transition time. Lastly, we found that the time decays like a power law with the speed v_0 of the Vicsek model and the number of steps m of the reactions.

Furthermore, while the investigation of chirality and the question how homochirality emerges was the motivation and starting point of this investigation, we note that the model we investigated is more general. Since the chirality of the particles does not enter the equations of motion, that is the equations of motion are the same for left- and right-chiral particles, the model can be more generally considered a model for the competition and spread of an arbitrary property in a population of particles interacting through alignment interactions. On the other hand, there is evidence that the chirality of cells influences their spatial dynamics in that the left-chiral and right-chiral cells move differently in space [122, 138, 240, 243]. Thus, a natural extension of the model above is to extend it to account for chirality-dependent spatial dynamics. Furthermore, to compare the theoretical model discussed here with experiments, using cells is rather hard. Experiments using bacteria,

some of which have been both successfully described using the Vicsek model and shown to be chiral might thus be better suited to test some of the predictions made above. Finally, an analytical theory of the model we simulated could be developed along the lines of the model of Jafarpour et al. [231, 236]. A stochastic differential equation for the order parameter can be derived from the reaction rates. The main difficulty of generalizing this approach to our model consists in including the anisotropic, non-equilibrium spatial dynamics.